JOURNAL OF Materials CHEMISTRY

Structural study of zinc-substituted nickel hydroxides

Cécile Tessier,[a,b] Liliane Guerlou-Demourgues,[a] Christiane Faure,[a] Alain Demourgues[a] and Claude Delmas[a]

[a]*Institut de Chimie de la Matière Condensée de Bordeaux-CNRS and Ecole Nationale Supérieure de Chimie et Physique de Bordeaux, Av. Dr. A. Schweitzer, 33608 Pessac CEDEX, France; E-mail: delmas@icmcb.u-bordeaux.fr; Fax: (33) 5 56 84 66 34; Tel: (33) 5 56 84 62 96*

[b]*SAFT - Direction de la Recherche, 111-113 boulevard Alfred Daney, 33074 Bordeaux CEDEX, France*

Received 26th October 1999, Accepted 2nd February 2000

The structure of zinc-substituted nickel hydroxide is investigated as a function of the amount of zinc. The hydroxide shows a β-type structure with up to 10% zinc in substitution for nickel (in mol), whereas an α-type phase is stabilised with 20–50% zinc. For the β-type phases, the unit cell parameters are similar to those of the non-substituted phase. The X-ray diffraction patterns evidence the presence of stacking faults. Zinc cations are located in octahedral sites of the slab in substitution for nickel. For the α-type phases ($d_{interslab} = 8.4$ Å), EXAFS spectroscopy gives evidence that the zinc cations are located in tetrahedral sites of the interslab space, these tetrahedra share one face with the octahedral vacancies within the slab. Mass spectrometry coupled with thermogravimetric analysis together with chemical analysis show the presence of carbonate ions in this phase. These anions are monodendate as evidenced by IR spectroscopy. The existence of pairs of zinc cations located above and below the octahedral vacancies of the slab can be considered. This implies an excess of positive charge which is compensated by the intercalation of carbonate ions. However, the turbostratic character of the α-type phase allows the coexistence of other local configurations within the structure.

Introduction

Nickel hydroxide is widely used as the active material in the positive electrode of Ni/Cd, Ni/MH and Ni/H_2 batteries. Various elements are commonly substituted for nickel to improve the electrochemical behaviour of the electrode; among them, zinc has been intensively studied. The main reported effect of zinc consists in preventing the formation of the γ-phase upon overcharge in concentrated electrolyte.[1–7] In order to clarify the reason for this effect, which remains unclear, a systematic structural study of the zinc-substituted nickel hydroxides was undertaken.

Before studying zinc-substituted nickel hydroxide, let us briefly recall the structure of non-substituted nickel hydroxides. Two varieties are generally considered. The first one, β(II)-$Ni(OH)_2$, crystallises in the trigonal system (space group: $P\bar{3}m1$), the indexation of the X-ray diffraction pattern being therefore performed with hexagonal axes. Its structure can be described as a packing, along the *c*-axis, of NiO_2 slabs made of edge-sharing NiO_6 octahedra. Protons are located in tetrahedral sites in the interslab space, just below and above the oxygen atoms. Actually, as recently reported, stacking faults are always present in the material obtained by precipitation.[8–10] There is no long range ordering but it is possible to consider a hexagonal cell in first approximation. The a_{hex} and c_{hex} cell parameters can be calculated from the positions of the (110) and (001) lines, respectively. Their values (3.13 Å and 4.61 Å) correspond to the Ni–Ni distance within the slab and to the interslab distance, respectively. Nickel hydroxide also exists in a hydrated form, named α-$Ni(OH)_2$. Its structure derives from that of the β(II)-$Ni(OH)_2$ phase by intercalation of one layer of water molecules as well as of anions into the interslab space. Generally, the α-phase presents a turbostratic structure:[11] the slabs are all equidistant and perpendicular to the *c*-axis, but they are misoriented with respect to one another. Such a structure leads to a very characteristic X-ray diffraction pattern. By analogy with the β-hydroxide, the first line at low angles is therefore denoted (001), this allows the determination of the interslab distance (≈8 Å). The broad and asymmetric (10*l*) and (11*l*) bands allow the determination of the Ni–Ni distance within the slab (3.08 Å) corresponding to a pseudo-"a_{hex}" cell parameter. An ordered structure exhibiting ABBCCA oxygen packing, named α*-$Ni(OH)_2$, was obtained by "chimie douce" reaction starting from sodium nickelate.[12]

In order to get a deeper insight into the role of zinc in these materials, we have undertaken a general study of zinc-substituted nickel hydroxide. The results concerning the chemical and structural characterisation are reported in the present paper. An investigation of these materials was very recently reported by Dixit *et al.*[13] These authors proposed a relevant structural model based on its similarity with the hydrozincite structure[14] but without any experimental proof. In battery applications, a few percent of zinc are generally substituted for nickel in the active material; in the present work, a general investigation from 0 to 50% zinc was carried out in order to have a more general overview of the effect of zinc. As shown in the following, the poor crystallinity of these materials makes a structural characterisation difficult. Therefore, a compilation of the data collected from several methods (X-ray diffraction (XRD), IR spectroscopy, X-ray absorption (XAS), chemical analysis and thermogravimetric analysis (TGA)) was necessary to propose a structural model.

Experimental

Zinc-substituted nickel hydroxides were obtained by precipitation: 200 ml of a 1 M metal salt solution ($NiSO_4$ and $ZnSO_4$ in the appropriate ratio) were dropped into 300 ml of a 2 M NaOH solution at 25 °C. The pH value was thus maintained equal to 14 all along the precipitation. The precipitate was then

DOI: 10.1039/a908517c

washed with deionised water until the wash water was at a steady pH of 8–9, it was then dried for 15 h at 60 °C.

XRD patterns were obtained with a Siemens D5000 diffractometer (Cu K_α). They were recorded with a scan step of 0.04°(2θ) for 25 s.

Chemical analyses were performed either by inductively coupled plasma (ICP) for Ni and Zn or by elementary organic microanalysis for C and H at the Vernaison Analysis Center of CNRS.

TGA were performed with a Setaram TGDTA92 thermogravimetric analyser at a rate of 2 °C min^{-1} in air from room temperature to 500 °C with a final thermal plateau at this temperature for 1 h. Gases evolving during TGA were analysed by a quadripolar Balzers Thermostar mass spectrometer.

IR spectra were recorded on a Perkin-Elmer Spectrum One spectrometer in the 400–4000 cm^{-1} range. The powder was dispersed in acetone and one drop was deposited on a CsI disk. The spectra were recorded after evaporation of the acetone.

The X-ray absorption measurements were carried out on beam line XAS4 at the Laboratoire pour l'Utilisation du Rayonnement Electromagnétique (LURE) in Orsay (France). Nickel and zinc K absorption edges (8333 eV and 9659 eV, respectively) were investigated. A Si(311) monochromator was used for energy selection. For both cases, a scan of the energy was performed from 100 eV below to 1000 eV above the edges. All the experiments were performed at 4.2 K.

Results

In the following, the various materials are designated by their structural type (β or α) followed by the Zn/(Ni+Zn) atomic ratio (expressed in percentage) used in the synthesis.

X-ray diffraction study

Fig. 1 shows the X-ray diffraction patterns of the 6–50% zinc-substituted nickel hydroxides. For 6 and 10% zinc, the X-ray diagram of the material corresponds to the β(II)-$Ni(OH)_2$ phase commonly obtained in these experimental conditions. The unit cell parameters ($a_{hex}=3.13$ Å, $c_{hex}=4.66$ Å) are similar to those of the non-substituted phase. The abnormal broadening of the (101) and (102) diffraction lines indicates the presence of a large amount of stacking faults.[8,9]

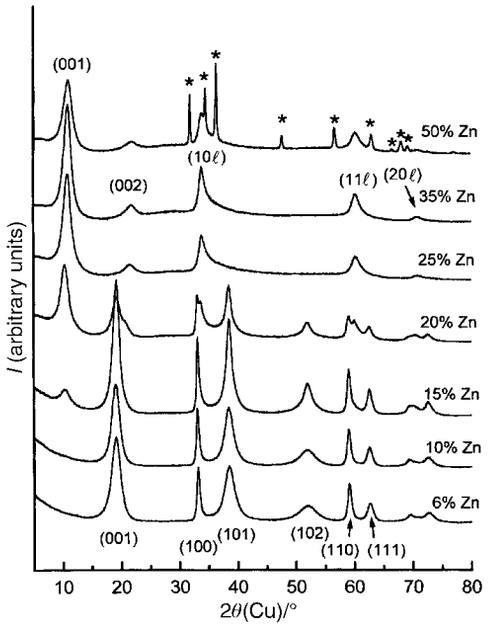

Fig. 1 XRD patterns of zinc-substituted nickel hydroxides obtained by precipitation at 25 °C and drying at 60 °C for increasing amounts of zinc, ranging from 6 to 50%. For the material with 50% zinc, the "*" symbol characterises lines of the ZnO phase.

From 15% zinc onward, a new phase appears; the $2\theta=10.5°$ diffraction line is characteristic of an α-$Ni(OH)_2$-type phase. For 25 and 35% zinc, a pure α-type phase is obtained. Its X-ray diffraction pattern (Fig. 1) shows two asymmetric and broad bands ($2\theta\approx34°$ and $2\theta\approx60°$) which are characteristic of a turbostratic structure. The Ni–Ni distance within the slab is equal to 3.08 Å as expected for an α-type phase and the interslab distance is equal to 8.4 Å. One has to notice that the intensity ratio between the (001) and (002) lines is higher for the zinc-substituted α-phase than for a non-substituted one, which suggests a slight difference in the cationic distribution of the two materials.

From 50% zinc onward, diffraction lines for the ZnO zincite phase appear together with lines of the α-type phase. This amount of zinc is thus beyond the solid solution domain of the α-type phase.

This study indicates the stabilisation of an α-type phase by zinc cations beyond 20% substitution, in agreement with the results of Ezhov and Malandin.[1] In fact, the limit composition between β- and α-type phases is sensitive to the drying conditions: if the material is dried at 90 °C, a pure β(II)-type phase is obtained for 15% of zinc. This limit composition between the β- and the α-phases is slightly different from that found by Dixit *et al.*;[13] actually, these authors used different precipitation conditions (lower pH, the presence of Na_2CO_3), which favour the formation of the α-phase. We further characterised the two kinds of materials with, respectively, α- and β-type structures. The β-type phase was expected to be a solid solution of zinc-substituted nickel hydroxide and the present study aimed at checking that zinc cations are located in octahedral sites in substitution for nickel in this structure. However, the main point of this study was to investigate the α-type phase, the formation of which was unexpected in the synthesis conditions used.

Elemental chemical analysis

Molar ratios of nickel, zinc, carbon and hydrogen in the phases with 6, 10, 25 and 35% zinc are given in Table 1. For each material, the Zn/(Ni+Zn) ratio is very close to that present in the sulfate parent solutions (indicated in the "Sample" column). In the β-type phases, the H/(Ni+Zn) molar ratio is higher than 2, which indicates the presence of adsorbed water molecules. The H amount is typically higher in the α-type phases than in the β-type ones, which is in agreement with the presence of water molecules in the interslab space of the α-type phases.

In the zinc-substituted β-phases, the amount of carbon (carbonate ions) is, surprisingly, twice that present in non-substituted β-phases. This amount is still strongly increased in α-type phases.

Thermogravimetric analysis

The thermogravimetric analysis curves of the $\beta_{10\%\ Zn}$ and $\alpha_{25\%\ Zn}$ phases are shown in Fig. 2 and Fig. 3a, respectively. They both exhibit a two-step weight loss separated by a well-defined plateau in the 180–200 °C range. In the case of the β-hydroxide, the data reported in the literature suggest that there is only desorption of water in the first step, while above 220 °C, the hydroxide slabs are decomposed leading to an $Ni_{1-y}Zn_yO$-type oxide (NiO structural type).[15,16] In the case of the α-system, the first weight loss is classically attributed to the evolution of adsorbed water but also of a part of the intercalated water, as reported for the first time by Le Bihan and Figlarz[15] and later by Faure *et al.*[17,18] Therefore, the first weight loss is higher for the α-type materials than for the β-type ones.

Mass spectrometry was coupled with TGA in the case of the $\alpha_{25\%\ Zn}$ phase. The variations of the ionic current correspond-

Table 1 Values of the A/(Ni+Zn) (A = Ni, Zn, C, H) molar ratios for various elements in zinc-substituted nickel hydroxide with 6–35% zinc. For the $\alpha_{25\%\ Zn}$ phase, the elemental chemical analysis is also reported after thermal treatment at 200 °C. The Zn/(Ni+Zn) ratio in sulfate mother solution is indicated in the "Sample" column

Sample	Ni/(Ni+Zn)	Zn/(Ni+Zn)	C/(Ni+Zn)	H/(Ni+Zn)
$\beta_{6\%\ Zn}$	0.94	0.06	0.08	2.37
$\beta_{10\%\ Zn}$	0.90	0.10	0.08	2.35
$\alpha_{25\%\ Zn}$	0.76	0.24	0.16	3.46
$\alpha_{35\%\ Zn}$	0.66	0.34	0.12	3.13
$\alpha_{25\%\ Zn}$–200 °C	0.76	0.24	0.15	2.51

ing to the CO_2^+, OH^+ and H_2O^+ ionic species *vs.* temperature are reported in Fig. 3b. This figure clearly shows that only H_2O is removed below 200 °C. X-ray diffraction of the material obtained by TGA on the 200 °C plateau shows that the turbostratic structure is preserved (Fig. 4). The interslab distance has decreased from 8.4 Å down to 7 Å, in good agreement with the general behaviour of α-type nickel hydroxides. Comparison of the chemical analysis of the material obtained at 200 °C with that of the starting material (Table 1) indicates a significant decrease in the H/(Ni+Zn) molar ratio in good agreement with mass spectrometry. All these results confirm that the decrease in the interslab distance with temperature during the first weight loss results from a partial loss of intercalated water.

Above 220 °C, the mass spectrometry experiment shows an H_2O evolution immediately followed by an H_2O+CO_2 one. In addition, the material obtained at 500 °C at the end of the TGA experiment is a mixed $Ni_{1-y}Zn_yO$ phase. It seems that, in a first step, the remaining water begins to be deintercalated. This is immediately followed by simultaneous dehydroxylation and decarbonatation of the material during the decomposition of the slabs.

IR spectroscopy

IR spectra of the $\beta_{10\%\ Zn}$ and of the $\alpha_{25\%\ Zn}$ phases are shown in Fig. 5 and 6, respectively. These spectra are comparable with those obtained by Dixit *et al.* for aged (β-type) and as-prepared (α-type) nickel–zinc hydroxides, respectively.[13] Three frequency domains can be considered. The first one, ranging from 400 to 800 cm^{-1} corresponds to lattice vibrations. In the second one, between 800 and 1500 cm^{-1}, vibrations of adsorbed or intercalated species can be found. The vibrations of the third domain, between 1500 and 4000 cm^{-1} give information about the hydration state of the phase and more especially the presence or not of intercalated (structural) water.

The IR spectrum of the zinc-substituted β(II)-hydroxide is very similar to those of non-substituted hydroxides.[19] Three bands can be seen, the two at 440 and 510 cm^{-1} can be attributed to ν(Ni–O) and δ(O–H) vibrations, respectively. The intense and sharp band at 3630 cm^{-1} corresponds to the ν(O–H) stretching mode and is characteristic of free hydroxy groups, *i.e.*, groups that are not involved in hydrogen bonds. As expected for a β(II)-hydroxide, there is no intense band that

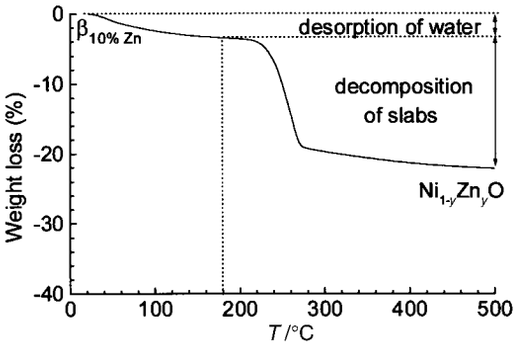

Fig. 2 TGA curve of the $\beta_{10\%\ Zn}$ phase (heating rate: 2 °C min^{-1} in air).

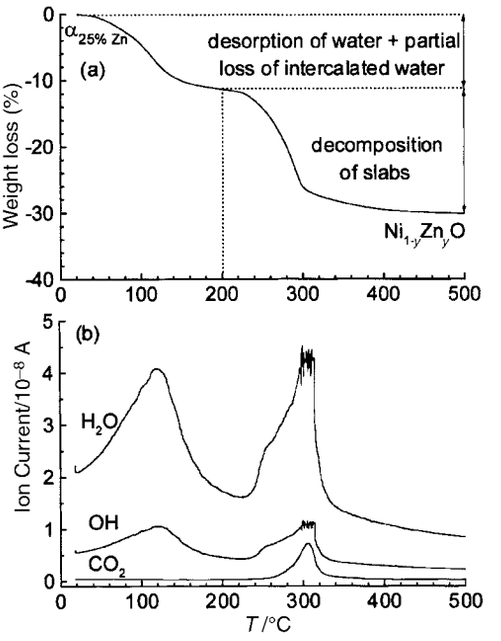

Fig. 3 (a) TGA curve of the $\alpha_{25\%\ Zn}$ phase (heating rate: 2 °C min^{-1} in air). (b) Curve of the mass spectrometry analysis coupled with TGA for the $\alpha_{25\%\ Zn}$ phase.

would correspond to intercalated species in the 800–1500 cm^{-1} range. Nevertheless, the very weak bands in this domain can be attributed to the adsorbed CO_3^{2-} anions evidenced by chemical analysis (Table 1).

For the α-type phase, the bands at 465 and 615 cm^{-1} are attributed to ν(Ni–O) and δ(O–H) vibrations, respectively. These bands have higher energies than those of the β(II)-type phase. The 4 bands at 845, 1050, 1345 and 1455 cm^{-1} are characteristic of the presence of carbonate ions. The presence of the ν_1 band (1050 cm^{-1}), together with the splitting of the ν_3 vibration mode into two bands indicates a lowering of the symmetry of the carbonate ion from the D_{3h} symmetry for the free species to either the C_{2v} or the C_s symmetry for the mono-

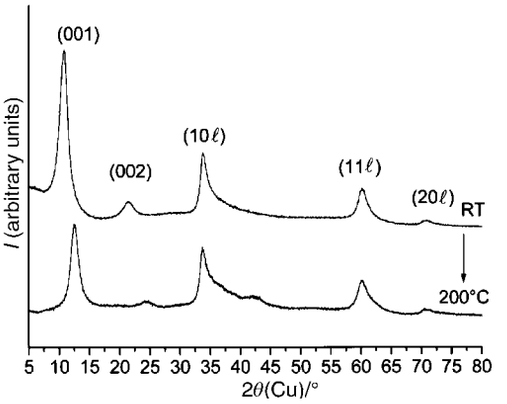

Fig. 4 Comparison of the XRD patterns of the $\alpha_{25\%\ Zn}$ phase at room temperature (RT) and after heating at 200 °C.

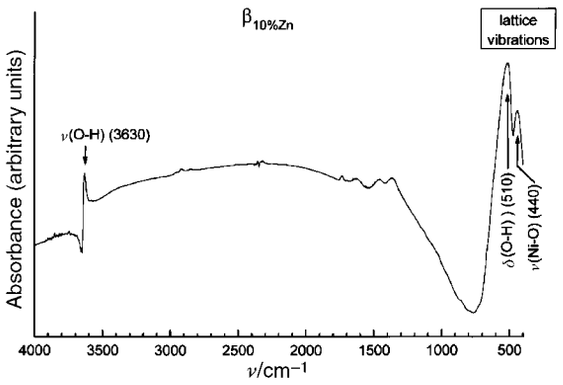

Fig. 5 IR spectrum of the $\beta_{10\%\ Zn}$ phase.

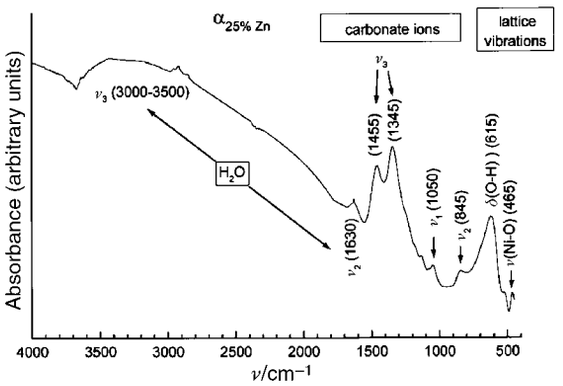

Fig. 6 IR spectrum of the $\alpha_{25\%\ Zn}$ phase.

or bidendate species, respectively. The 110 cm^{-1} energy difference between the two ν_3 bands (1345 and 1455 cm^{-1}) is related to a monodendate species, the splitting being closer to 300 cm^{-1} in the bidendate case.[20,21] Finally, the band at 1630 cm^{-1} and the broad band between 3000 and 3500 cm^{-1} can be attributed to structural water. Furthermore, the absence of the sharp band at 3630 cm^{-1} reveals the absence of free hydroxy groups: as expected for an α-type phase, the hydroxy groups are all hydrogen bonded with water molecules and carbonate anions. As reported by Figlarz and Le Bihan,[19] these hydrogen bonds lead to a shift to higher energy values of the ν(Ni–O) and δ(O–H) bands in the α-phase *vs.* the β-type one, as previously mentioned.

IR spectroscopy allows the confirmation of the X-ray diffraction conclusions concerning the β- or α-structural type. It is also in good agreement with the results from the chemical analysis and the mass spectrometry coupled with TGA since the three techniques evidence the presence of carbonate ions in the α-phase. Moreover, it shows that carbonate ions are linked only by one of their oxygen atoms to the nickel or zinc ions.

X-ray absorption spectroscopy

In order to try to determine the local environment of zinc in both structures, the β- and α-zinc-substituted phases were characterised by X-ray absorption.

Zn K-edge X-ray absorption near edge structure (XANES) study. The Zn K-edge spectra of the $\alpha_{25\%\ Zn}$ phase and of the $\beta_{10\%\ Zn}$ phase can be compared in Fig. 7. One has to notice that no pre-edge peak can be seen in either case. Depending on the local symmetry, pre-edge absorption peaks can indeed be observed for 3d transition elements, due to dipole transition to p-like states admixed to 3d states.[22] As the 3d shells in zinc compounds are completely filled, no pre-edge absorption peak is expected whatever the zinc environment.

Meanwhile, the absorption peak is significantly broader in the case of the α-phase than in the case of the β-phase. Hennig *et al.*[22] and Takahashi *et al.*[23] showed, for zinc-based complexes, that the shape of the white line depends on the local environment. They reported a broadening of the peak when the zinc coordination number decreased from 6 to 4. Such an effect can be related to the increase in covalency of the Zn–O bond. On the basis of these results, the experimental spectra presented in Fig. 7 suggest that zinc cations are located in tetrahedral sites in the α-phase and in octahedral sites in the β-phase. Moreover, the shape of the XANES spectrum of the α-phase is similar to that reported by Choy *et al.* for (Ni,Zn)-acetate layered hydroxides,[24] where zinc cations were reported to be located in tetrahedral sites.

Extended X-ray absorption fine structure (EXAFS) study. The α-type phase was investigated at both the Zn and Ni K-edges, while only the Zn K-edge was studied for the β-phase. Indeed, a study of the Ni K-edge for the latter phase was not expected to be relevant as a result of the insufficient amount of zinc in this material to induce significant changes on the nickel environment.

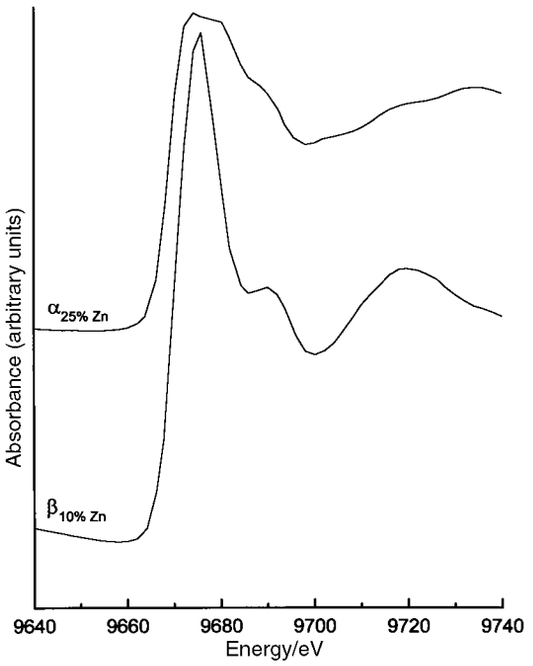

Fig. 7 Comparison of the Zn K-edge XANES spectra of the $\alpha_{25\%\ Zn}$ phase and of the $\beta_{10\%\ Zn}$ phase. The two spectra were normalised in order to have the same signal amplitude difference between the minima before and after (around 9700 eV) the white line.

X-ray absorption spectra at the Ni and Zn K-edges were reduced to normalised XAFS $\chi(k)$ using DARESBURY software and weighted $k^3\chi(k)$ data were analysed using the EXCURV suite of programs.[25,26] Least squares analyses against model environments were enabled by employing a theoretical phase shift and a backscattering amplitude that were calculated and compared with the NiO and ZnO oxides as reference compounds. The parameters that take into account inelastic losses, the core hole lifetime and also the scale factor accounting for the non-unity quantum efficiency of the absorption process were refined in the case of NiO and ZnO. From a general point of view, good quality spectra were obtained up to $k = 14$ $Å^{-1}$, leading to a maximum separation of bond distances on the Fourier transform equal to 0.16 Å ($\Delta R = \pi/2\Delta k$, $k_{min} = 4$ $Å^{-1}$, $k_{max} = 14$ $Å^{-1}$). In the case of the $\beta_{10\%\ Zn}$ phase at the Zn K-edge, the maximum limit of the spectrum was set at $k_{max} = 12$ $Å^{-1}$, leading in this case to a maximum separation of bond distances equal to 0.20 Å; in addition, the signal-to-noise ratio of the EXAFS oscillations

was too low to enable a refinement of more than two shells. A gaussian window was used for the Fourier transform. The usual fitting index FI is defined by:

$$\sum_i [(1-\sigma_i)(\chi_{i,\mathrm{exp}}-\chi_{i,\mathrm{theor}})]^2$$

where i ranges over all the points in the spectrum, σ_i is given by

$$1/\sigma_i = k_i^3 / \sum_j k_j^3 |\chi_{j,\mathrm{exp}}|$$

and χ_i is the reduced EXAFS function. It is worth noting that in the case of materials such as ours an FI value of 0.0003 or less corresponds to a good fit.[25,26]

Refinement of the EXAFS data was performed by systematically considering in a first step an oxygen shell surrounding nickel or zinc. The refinement was then improved by gradually adding the subsequent shells (comprising nickel or zinc neighbours). Since the co-ordination numbers and the Debye–Waller factors are strongly correlated, the co-ordination numbers were first fixed at given values and the Debye–Waller factors, the distances and the energy shift were refined on this basis. The relevance of the Debye–Waller factors and distances thus obtained allowed us to validate the co-ordination numbers initially chosen.

Study of the $\beta_{10\%\ Zn}$ phase at the Zn K-edge. The $k^3\chi(k)$ EXAFS signal of the $\beta_{10\%\ Zn}$ phase, as well as the corresponding Fourier transform are represented in Fig. 8. Two shells corresponding, respectively, to the oxygen and nickel (or zinc) first and second neighbours are clearly evidenced on the Fourier transform.

Refinement of the experimental data leads to the conclusion that zinc cations are located in an octahedral environment with 6 oxygen atoms at 2.03 Å and that they have 6 nickel (zinc) neighbours at 3.11 Å. This is in good agreement with structural features of non-substituted nickel hydroxides obtained by Pandya *et al.*,[27] Cornilsen *et al.*,[28] and Mansour and Melendres[29] *via* EXAFS spectroscopy. The Zn–O distance is slightly smaller than the sum of the ionic radii of divalent zinc in an octahedral environment and oxygen ($r_{Zn^{2+}} = 0.74$ A, $r_{O^{2-}} = 1.40$ A) but is very close to the Ni–O distance in β-$Ni(OH)_2$, since zinc is substituted for nickel within the slab. The Zn–Ni distance corresponds to the cation–cation distance within the NiO_2 slab of a β(II)-type hydroxide (the average value determined from XRD is equal to 3.13 Å (a_{hex})). Nevertheless, the accuracy of the EXAFS study cannot absolutely exclude the presence of zinc cations in the interslab space. Actually, in the ideal structure (ABAB oxygen packing), the strong electrostatic repulsion must inhibit the presence of zinc within the octahedra of the interslab space. However, as there are some stacking faults in the structure, some of the octahedra of the interslab space share only one face (growth fault) or no face (deformation fault) with the $(Ni,Zn)O_6$ octahedra of the slabs.[9] Therefore, in this case, the electrostatic destabilisation is lowered (growth fault) or suppressed (deformation fault). As a result, it cannot be excluded that some zinc cations are located in octahedral sites in the interslab space in the vicinity of stacking faults.

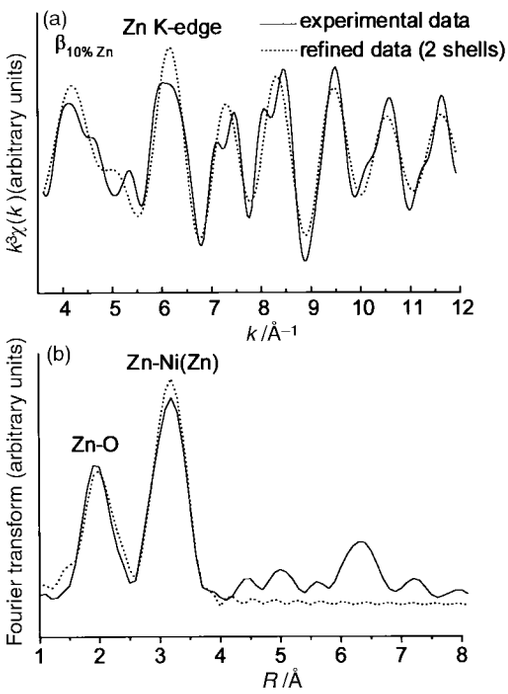

Fig. 8 (a) Zn K-edge EXAFS spectrum and (b) its Fourier transform for the $\beta_{10\%\ Zn}$ phase.

Study of the $\alpha_{25\%\ Zn}$ phase: at the Ni K-edge. The $k^3\chi(k)$ EXAFS signal obtained at the Ni K-edge for the α-phase as well as the corresponding Fourier transform are represented in Fig. 9. Four shells related to Ni–O and Ni–Ni(Zn) distances are clearly evidenced. Refinement of the EXAFS data leads to an Ni–O distance (2.04 Å for the first oxygen shell) and to Ni–Ni distances (3.06, 5.28 and 6.23 Å for the first three nickel shells) characteristic of nickel ions located in edge-sharing oxygen octahedra, in good agreement with the set of Ni–Ni distances expected in an NiO_2 slab on the basis of the a_{hex} parameter ($d_{Ni-Ni} = 3.13$, 5.42, 6.26 Å) and with previous studies.[27–29] The value of the FI fit index obtained for this refinement, *i.e.*, 0.00025 shows the goodness of the fit.

Nevertheless, it clearly appears that the Fourier transform calculated at the Ni K-edge on the basis of the oxygen and nickel shells mentioned above (curve with dashed line in Fig. 9b) does not match very well with the experimental curve (full line in Fig. 9b), since the latter exhibits a shoulder for distances around 3.50 Å which is not taken into account. The fitting will be improved after considering an additional zinc shell deduced from the results obtained at the Zn K-edge, which will be presented in the next section.

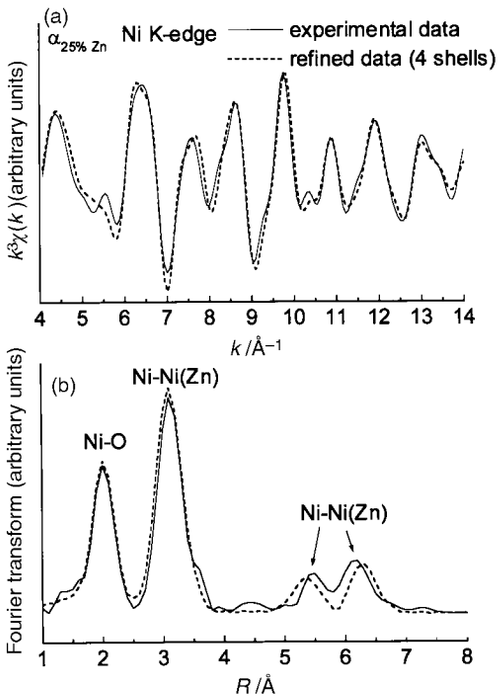

Fig. 9 (a) Ni K-edge EXAFS spectrum and (b) its Fourier transform for the $\alpha_{25\%\ Zn}$ phase. Four shells were used for the refinement: one 6-oxygen shell and three shells of 6 nickel (zinc) cations of the slab.

Study of the $\alpha_{25\%\ Zn}$ phase: at the Zn K-edge. The $k^3\chi(k)$ EXAFS signal obtained at the Zn K-edge as well as the corresponding Fourier transform are represented in Fig. 10 for the $\alpha_{25\%\ Zn}$ phase. The Fourier transform shows four main shells (one oxygen shell and three nickel (zinc) ones). In the first step, the octahedral and tetrahedral oxygen surrounding the zinc were successively considered for the refinement but the results show unambiguously that only the second model is relevant. The fixed and refined parameters corresponding to the best fit, *i.e.*, for zinc with tetrahedral oxygen surrounding, are given in Table 2. The corresponding FI index is equal to 0.00027, which corresponds to a good fit.

According to this refinement, the Zn–O distance is equal to 1.94 Å. This value is close to the sum of ionic radii of Zn^{2+} in tetrahedral environments and oxygen ($r_{Zn^{2+}} = 0.60$ A, $r_{O^{2-}} = 1.40$ A). Moreover, it is in full agreement with data reported elsewhere for zinc in tetrahedral surroundings in related structures.[14,24,30,31] The second shell is comprised of nickel ions located at 3.50 Å *vs.* Zn, which does not correspond to any distance within the NiO_2 slab. One can therefore assume that zinc cations are located within the interslab space. It should be noted that the presence of zinc with octahedral oxygen surrounding was also envisaged. For this purpose, we assumed the presence of 10% zinc in octahedral co-ordination (6 oxygen atoms at a distance of 2.04 Å from zinc) and 90% zinc in tetrahedral co-ordination (4 oxygen atoms at a distance of 1.94 Å from zinc). Starting from such a hypothesis, a refinement of the Zn–O distances and of the Debye–Waller factors led to a significant decrease of the Zn–O distance primarily fixed to 2.04 Å down to 1.94 Å while the Zn–O distance primarily fixed to 1.94 Å remained quite unchanged. Such a behaviour shows clearly the absence of any significant amount of zinc in octahedral co-ordination in addition to zinc in tetrahedral co-ordination.

As mentioned in the introduction, the α-type structure can be considered in first approximation as a packing of $Ni(OH)_2$ slabs separated by a layer of oxygen atoms belonging to water molecules and intercalated species (OH^-, CO_3^{2-}). Even if the structure exhibits a turbostratic character due to misorientation of the slabs, the oxygen packing can be considered at the local scale. Depending on the relative position of the oxygen atoms in the interslab space *vs.* the NiO_2 slab and on the upward or downward orientation of the tetrahedra, four different tetrahedral sites can be envisaged as shown in Fig. 11. In the first case (Fig. 11a), the tetrahedron shares three edges with three NiO_6 octahedra of the slab (ABA oxygen packing). In the second case (Fig. 11b), the tetrahedron shares one face with one octahedron of the slab (ABC oxygen packing). Two other possibilities can be considered, where the ZnO_4 tetrahedron shares one corner with three NiO_6 octahedra of the slab with an ABA (Fig. 11c) or an ABC (Fig. 11d) oxygen packing. The distances between the zinc cation and its nickel neighbours were calculated for the four models on the basis of the Ni–Ni and Ni–O distances determined from the EXAFS study at the Ni K-edge (3.06 Å and 2.04 Å, respectively). The four models lead to very different calculated distances between the zinc ion and its nickel neighbours, as indicated in Fig. 11: 2.54, 3.98, 5.02, 6.63 and 7.95 Å in the first case (Fig. 11a), 1.82, 3.56, 5.60 and 6.39 Å in the second (Fig. 11b) and 3.44, 4.61, 5.53 and 7.02 Å in the other two (Fig. 11c and d). The zinc–nickel distances obtained after refinement (3.50, 5.64 and 6.32 Å (Table 2)) unambiguously validate the second model (Fig. 11b). Nevertheless, the 1.82 Å distance was not found in the refinement. Therefore, in good agreement with the third Pauling rule, the packing of model (b) leads to the occurrence of a nickel vacancy within the octahedron that shares one face with the ZnO_4 tetrahedron.

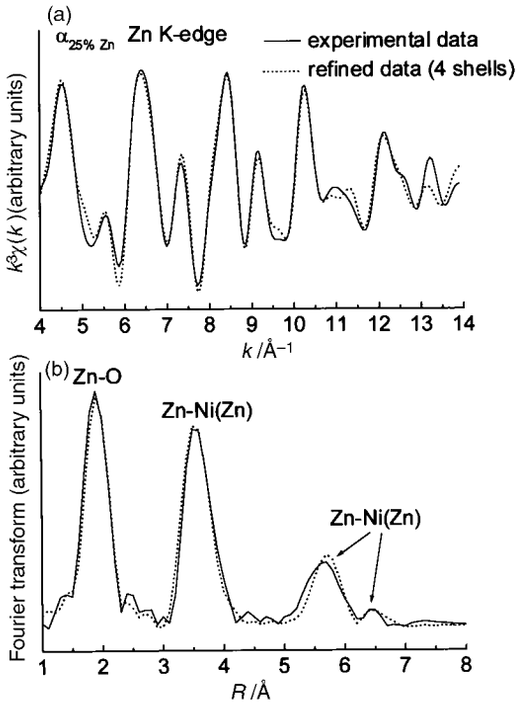

Fig. 10 (a) Zn K-edge EXAFS spectrum and (b) its Fourier transform for the $\alpha_{25\%\ Zn}$ phase.

Table 2 Parameters obtained after refinement of the EXAFS data at the Zn K-edge and at the Ni K-edge for the $\alpha_{25\%\ Zn}$ phase. The coordination numbers (CN) were fixed, whereas the distances from the absorbent atom (R) and the Debye–Waller factors $2\sigma^2$ were refined (the standard deviations are indicated in parentheses)

Edge	Shell	CN	R/Å	$2\sigma^2$/Å^2
Zn K-edge	Zn–O	4.0	1.94(1)	0.008
	Zn–Ni	6.0	3.50(1)	0.015
	Zn–Ni	6.0	5.64(1)	0.014
	Zn–Ni	6.0	6.32(1)	0.033
Ni K-edge	Ni–O	6.0	2.04(1)	0.010
	Ni–Ni	6.0	3.06(1)	0.011
	Ni–Ni	6.0	5.28(1)	0.019
	Ni–Ni	6.0	6.23(1)	0.010
	Ni–Zn	1.7	3.50(1)	0.015

As mentioned in the study at the Ni K-edge and illustrated in Fig. 9b, the experimental Fourier transform (full line in Fig. 9b) exhibits a shoulder around 3.50 Å which is not reproduced by the Fourier transform calculated at the Ni K-edge on the basis of the oxygen shell (6 neighbours) at 2.04 Å and of the three successive nickel shells (6 neighbours) at 3.06, 5.28 and 6.23 Å (curve with dashed line in Fig. 9b). Starting from this structural model, the EXAFS data obtained at the Ni K-edge were further refined by considering the presence of zinc ions in the tetrahedra of the interslab space. An additional shell comprised of 1.7 zinc neighbours (this value was calculated assuming the ideal cationic distribution

$$\underbrace{[Ni_{0.86}{}^{\square}{}_{0.14}]_{Oct}O_2}_{\text{Slab}}\ \underbrace{[Zn_{0.28}]_{Tetr}}_{\text{Interslab}}$$

which will be proposed in the following) at 3.50 Å (as obtained from the EXAFS study at the Zn K-edge) was considered. The refinement thus obtained leads to a rather good value of the Debye–Waller factor ($2\sigma^2 = 0.015$ Å^2) and entails as shown in Fig. 12a a significant improvement of the agreement between the calculated (dotted line) and the experimental data (full line). The fixed and refined parameters are given in Table 2.

This effect is even more obvious in the case of the $\alpha_{35\%\ Zn}$ phase, as shown by the comparison of the experimental and

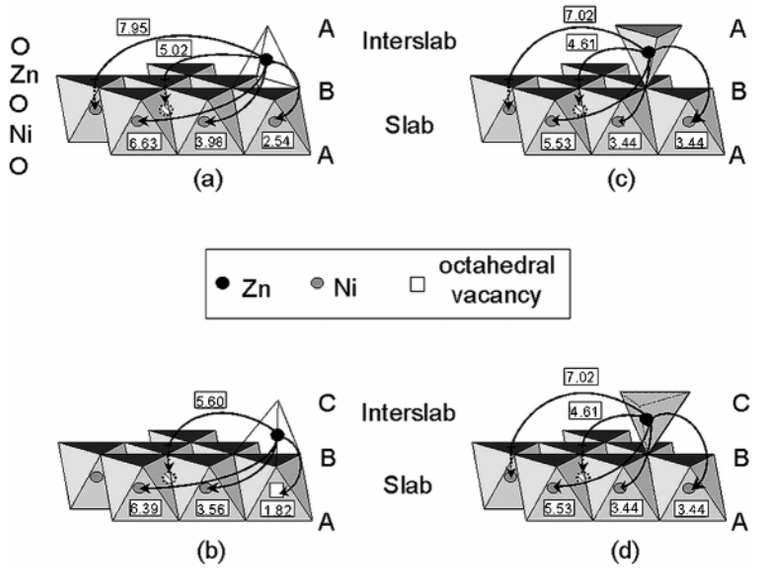

Fig. 11 Perspective view of one slab and one interslab space of the proposed structure of α-type zinc-substituted nickel hydroxide under the hypothesis that zinc cations are located in tetrahedral sites of the interslab space. Four different tetrahedral sites can be envisaged: the ZnO_4 tetrahedron shares three edges with three NiO_6 octahedra of the slab following an ABA oxygen packing (a) or alternatively, it shares one face with one octahedron of the slab following an ABC oxygen packing (b). Model (b) implies the occurrence of a nickel vacancy in the octahedron sharing one face with the ZnO_4 tetrahedron. The ZnO_4 tetrahedron can also share one corner with three NiO_6 octahedra of the slab with an ABA (c) or ABC (d) oxygen packing. Distances (in Å) between the zinc ion and its nickel neighbours or octahedral vacancy are indicated along arrows in the figure. Hatched circles indicate nickel atoms located in hidden octahedra in the background of the figure.

calculated Fourier transforms in Fig. 12b. The experimental Fourier transform exhibits at 3.50 Å a more intense shoulder than that observed in the case of the $\alpha_{25\%\ Zn}$ material. This peak cannot be modelled by considering only one oxygen shell and three nickel shells (the refinement in this case leads to the conclusion of the presence of 6 oxygen atoms at 2.04 Å and 6 nickel ions at 3.06, 5.28 and 6.23 Å) but is actually taken into account in considering for nickel 2.5 additional zinc neighbours at 3.51 Å (curve with dotted line in Fig. 12b). The value of 2.5 neighbours is calculated in a similar way as for the $\alpha_{25\%\ Zn}$ phase. Such a behaviour confirms again the relevance of model (b).

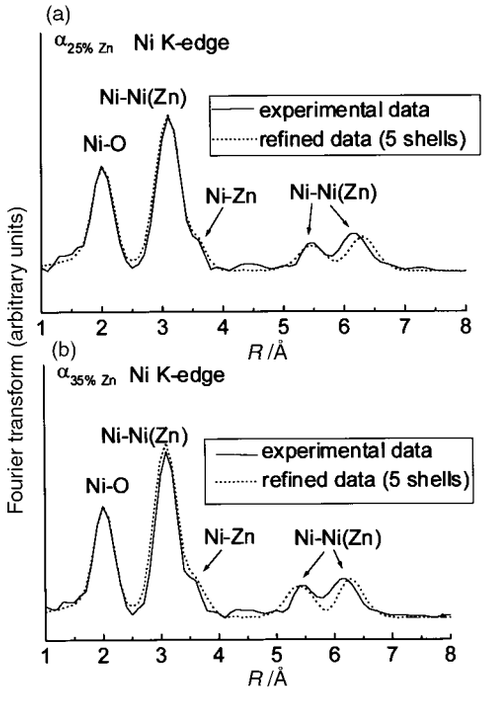

Fig. 12 (a) Ni K-edge Fourier transform of EXAFS oscillations for the $\alpha_{25\%\ Zn}$ phase and (b) for the $\alpha_{35\%\ Zn}$ phase. Five shells were used for both refinements: one 6-oxygen shell, three shells of 6 nickel (zinc) cations of the slab and an additional shell of zinc cations located in tetrahedral sites of the interslab space.

As previously reported by Pandya *et al.*,[27] it should be noted that the value of the Debye–Waller factor corresponding to the 6.23 Å Ni–Ni distance is smaller than that of the previous Ni–Ni shell at 5.28 Å, which is unexpected at first sight. This results from a strong focusing effect and a multiple scattering process due to the presence of linear Ni–Ni–Ni chains and it implies a significant increase of the Fourier transform amplitude for the Ni–Ni distance around twice the value of the "a_{hex}" cell parameter.

To sum up, the EXAFS data evidence the difference in site for zinc in the β- and α-phases, as illustrated by the comparison of the Fourier transforms in Fig. 13. For the α-type phase, the second shell clearly evidences that the zinc ions (d_{Zn-Ni} = 3.50 Å) are not located within the NiO_2 slab (d_{Ni-Ni} = 3.06 Å).

Discussion

The structure of zinc-substituted nickel hydroxide varies strongly with the amount of zinc. For a substitution of up to 10%, the structure is of the β-type as evidenced by X-ray

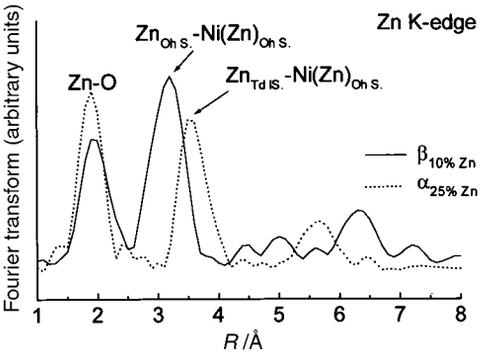

Fig. 13 Comparison of the Fourier transforms at the Zn K-edge of the α-type and of the β-type phases. Zinc cations in octahedral sites of the slab and in tetrahedral sites of the interslab space are denoted $Zn_{Oh\ S.}$ and $Zn_{Td\ IS.}$, respectively.

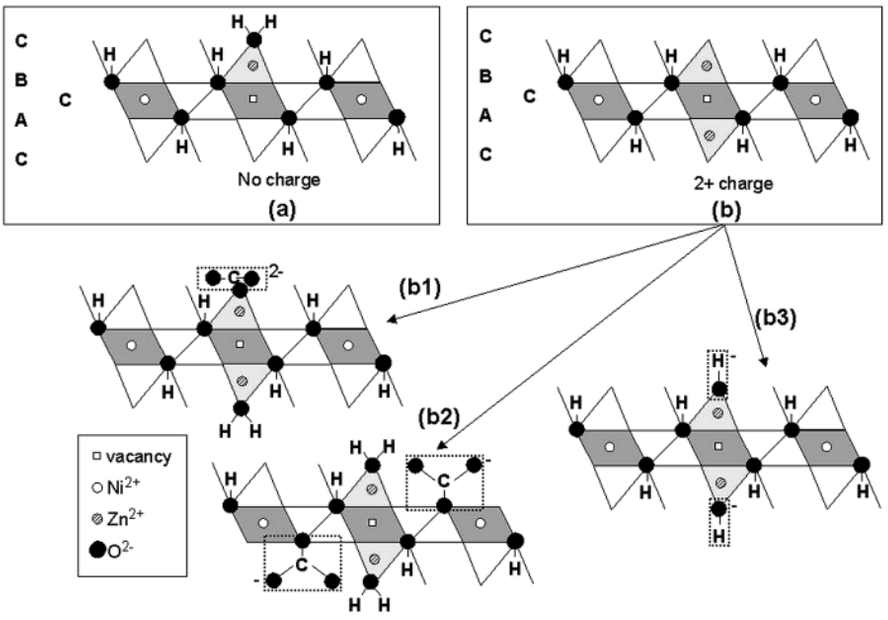

Fig. 14 Schematic representation of the structural configurations proposed to describe the structure of the $\alpha_{25\%\ Zn}$ phase. Section of the structure parallel to the (110) plane. In this description, the octahedra and tetrahedra are represented by parallelograms and triangles, respectively.

diffraction, thermoanalysis and IR spectroscopy. EXAFS spectroscopy allows the confirmation of the fact that the zinc cations are located in octahedral sites of the slab in substitution for nickel ions, as evidenced by the Ni–Zn distance being equal to the "a_{hex}" parameter. The rather close ionic radii of nickel and zinc cations in octahedral environment (0.69 and 0.74 Å, respectively[32]) enables the formation of a solid solution for small amounts of substituting elements, in good agreement with previous studies.[33]

Above 10% zinc substitution, however, an α-type structure appears and, for 25% zinc, a pure α-phase is obtained. For this α-type phase, EXAFS experiments allow the conclusion that zinc cations are located in tetrahedral sites of the interslab space. Moreover, each ZnO_4 tetrahedron shares one face with an empty octahedron of the slab. Chemical analysis, together with mass spectrometry coupled with TGA evidence the presence of carbonate ions in the structure. In addition, the IR spectrum of the α-type phase clearly shows that the carbonate ions are monodendate. They can be bonded either to a zinc or to a nickel cation. XRD evidences a turbostratic structure with an interslab distance of 8.4 Å. This distance is larger than that of layered double hydroxides with intercalated carbonate ions (7.7–7.9 Å) where anions are reported to lie parallel to the slabs.[18,34] Besides, an interslab distance of 8.4 Å excludes the intercalation of two monolayers of water between the slabs.

Several well-crystallised layered materials containing zinc were reported to present such a structure on the basis of a complete structural characterisation. The structure of hydrozincite, $Zn_5(OH)_6(CO_3)_2$, for instance, can be described as a packing of ZnO_2 layers made of edge-sharing ZnO_6 octahedra, but with 25% octahedral sites being unoccupied; above and under each of these vacancies are located two zinc cations in tetrahedral sites.[14] Each zinc cation in a tetrahedral site of the interslab space is bonded with three hydroxy groups of the nickel–oxygen slab and with an oxygen atom of a carbonate ion located in the interslab space This carbonate ion, oriented perpendicularly to the slab, is grafted to the next slab *via* a second oxygen atom, the third one being free. The resulting interslab distance has a value of 6.8 Å. Other phases are known to have a similar structure with zinc cations in both octahedral and tetrahedral sites: $Zn_5(OH)_6(NO_3)_2{\cdot}2H_2O$[31] and $Zn_5(OH)_6Cl_2{\cdot}H_2O$.[30] Their interslab distances (9.7 Å and 7.9 Å, respectively) are larger than that of hydrozincite because of the presence of water molecules in their interslab space. Finally, calcophanite, $ZnMn_3O_7{\cdot}3H_2O$,[35] presents a more unusual structure, with zinc cations in distorted octahedral sites in the interslab space: these cations have three short bonds with hydroxyl ions of the slab and three long bonds with intercalated water molecules. Nickel–zinc hydroxyacetates were reported for the first time by Yamanaka *et al.*[36] and later by Nishizawa and Yuasa.[37] The authors proposed a structure very similar to that which we describe in the present paper. More recently, this material was revisited by Choy *et al.*[24] who confirmed by an EXAFS study the model of Yamanaka *et al.* The three papers reported a turbostratic structure for this material and the location of some zinc cations in tetrahedral sites of the interslab space. Very recently, Dixit *et al.*[13] proposed a hydrozincite-type structure for zinc-substituted nickel hydroxides. In fact, the structural model proposed by these authors must be considered only at the local scale due to the turbostratic character of the structure.

On the basis of our results, two cationic distributions can be envisaged at the local scale for model (b) of Fig. 11: (i) one ZnO_4 tetrahedron sharing a face with a $\square O_6$ octahedron of the slab and (ii) two zinc cations located on both sides of the slab in tetrahedra sharing a face with the same $\square O_6$ octahedron. These two possibilities are shown schematically in Fig. 14a and b which present a section of the structure parallel to the (110) plane. In this description, the octahedra and tetrahedra are represented by parallelograms and triangles, respectively.[9] In both cases, each ZnO_4 tetrahedron shares three corners with the first three-neighbour NiO_6 octahedra. The hydrogen atoms that are bonded to the corner oxygen atoms are located in tetrahedra sharing one edge with a ZnO_4 tetrahedron. This implies a strong electrostatic repulsion between H^+ and Zn^{2+} cations. Therefore, one can assume that these protons are destabilised in their site.

In the first cationic distribution (Fig. 14a), the configuration implies no charge in excess, since an extra Zn^{2+} cation is associated with an Ni^{2+} vacancy. Therefore, no additional anion is required for electroneutrality. If some carbonate anions were located in the vicinity of this zinc cation, they would necessarily be bidendate to ensure electroneutrality, which is obviously not the case as evidenced by IR spectroscopy. Furthermore, one can assume that the oxygen atom of the ZnO_4 tetrahedron that is located at the C site in the interslab space belongs to a water molecule. If this oxygen did

belong to a monodendate carbonate anion, the two negative charges would indeed be in excess.

In the second cationic distribution (Fig. 14b), two zinc cations are located on both sides of the octahedral vacancy of the slab, which implies a 2+ excess of charge. To ensure electroneutrality, intercalation of anions is required: carbonate ions (Fig. 14b1 and 14b2) or hydroxyl ions (Fig. 14b3). If carbonate ions are bonded to zinc ions of the interslab space (Fig. 14b1), each anion brings a 2− charge excess. Therefore, for each pair of zinc cations, only one of them is bonded to a carbonate ion, whereas the second one is bonded to the oxygen atom of an intercalated water molecule. This model leads to a C : Zn molar ratio equal to 1 : 2. If carbonate ions are bonded to nickel ions (Fig. 14b2), each carbonate ion replaces one hydroxy group, which leads to a 1− charge excess. Therefore two carbonate ions bonded to nickel ions are required to ensure electroneutrality in the vicinity of a pair of zinc cations. This implies a C : Zn molar ratio of 1. Hydroxyl ions can also be bonded to zinc cations in the interslab space (Fig. 14b3): two hydroxy groups are required for each pair of zinc cations.

The experimental C : Zn ratio is equal to 2 : 3. Therefore, the structure can be reasonably described with a mixture of the two configurations modelled in Fig. 14b1 and 14b2. However, the other two possibilities cannot be totally excluded since the turbostraticity of the material evidences a structural disorder which allows the existence of several configurations within the structure. This questions the relevance of any chemical formula. Nevertheless, if one assumes a model involving a mixture of the local distributions represented in Fig. 14b1 and 14b2 to describe the structure of the zinc-substituted α-type phase, the distribution with two ZnO_4 tetrahedra sharing one face with the same $\square O_6$ octahedron of the slab (Fig. 14b) leads to the following cationic distribution in the case of the $\alpha_{25\%\ Zn}$ phase:

$$\underbrace{[Ni_{0.86}\square_{0.14}]_{Oct}O_2}_{\text{Slab}}\ \underbrace{[Zn_{0.28}]_{Tetr}}_{\text{Interslab}}$$

It should be noticed that, in the latter model, one Zn–Zn radial distance at 3.64 Å is expected on the Fourier transform of the Zn K-edge EXAFS signal. This distance is close to the 3.50 Å one corresponding to the nickel shell, so that it is impossible to separate the two shells.

Conclusion

This work shows that the α-type phase is stabilised by substituting increasing amounts of zinc for nickel in nickel hydroxide. Indeed, for up to 10% zinc, the β-structure is maintained, with zinc cations located in octahedral sites of the slab, whereas a pure α-type phase is obtained for 25 and 35% zinc, with zinc cations located in tetrahedral sites of the interslab space. The turbostraticity of the structure prevents any precise structural determination. Instead, several configurations can possibly exist in the material and among them the existence of pairs of zinc cations, on both sides of octahedral vacancies of the slabs, responsible for a 2+ charge excess. This charge excess is compensated by the intercalation between the slabs of carbonate ions linked by one of their oxygens to nickel or zinc cations.

The determination of the structure of this α-type zinc-substituted nickel hydroxide should allow an understanding of the improvement of the electrochemical behaviour of nickel hydroxide with zinc substitution. Further experiments including ageing tests in concentrated KOH, chemical and electrochemical cycling are in progress. They will be the subject of future publications.

Acknowledgements

We wish to thank M. Ménétrier, C. Audry and P. Bernard for fruitful discussion, L. Rabardel and D. Denux for their contribution to the TGA measurements and subsequent interpretation, as well as M. Basterreix, B. Delatouche and C. Denage for their technical support. We gratefully acknowledge the help of the staff of LURE, and more especially V. Briois. We are also grateful to SAFT and ANRT for financial support.

References

1 B. B. Ezhov and O. G. Malandin, *J. Electrochem. Soc.*, 1991, **138**, 885.
2 M. Oshitani, K. Takashima and Y. Matsumara, *Proc. Electrochem. Soc.*, 1990, **90-4**, 197.
3 M. Oshitani, T. Takayama, K. Takashima and S. Tsuji, *J. Appl. Electrochem.*, 1986, **16**, 403.
4 M. Oshitani, M. Watada, T. Tanaka and T. Iida, *Proc. Electrochem. Soc.*, 1994, **94-27**, 303.
5 M. Oshitani, H. Yufu and K. Hasegawa, *Eur. Pat.*, 89303952.9, 1989.
6 D. H. Fritts, *Proc. Electrochem. Soc.*, 1982, **82-4**, 175.
7 A. Yuan, S. Cheng, J. Zhang and C. Cao, *J. Power Sources*, 1999, **77**, 178.
8 C. Delmas and C. Tessier, *J. Mater. Chem.*, 1997, **7**, 1439.
9 C. Tessier, P. H. Haumesser, P. Bernard and C. Delmas, *J. Electrochem. Soc.*, 1999, **146**, 2059.
10 Z. S. Wronski, G. J. C. Carpenter, D. Martineau and P. J. Kalal, *Proc. Electrochemical Soc.*, 1997, **97-18**, 804.
11 S. Le Bihan, J. Guenot and M. Figlarz, *C. R. Seances Acad. Sci., Ser. C*, 1970, **270**, 2131.
12 J. J. Braconnier, C. Delmas, C. Fouassier, M. Figlarz, B. Beaudouin and P. Hagenmuller, *Rev. Chim. Miner.*, 1984, **21**, 496.
13 M. Dixit, P. Vishnu Kamath and J. Gopalakrishnan, *J. Electrochem. Soc.*, 1999, **146**, 79.
14 S. Ghose, *Acta Crystallogr.*, 1964, **17**, 1051.
15 S. Le Bihan and M. Figlarz, *Thermochim. Acta*, 1973, **6**, 319.
16 W. Dennstedt and W. Löser, *Electrochim. Acta*, 1971, **16**, 429.
17 C. Faure, C. Delmas, C. Fouassier and P. Willmann, *J. Power Sources*, 1991, **35**, 249.
18 C. Faure, C. Delmas and P. Willmann, *J. Power Sources*, 1991, **35**, 263.
19 M. Figlarz and S. Le Bihan, *C. R. Seances Acad. Sci., Ser. C*, 1971, **272**, 580.
20 C. Faure, Y. Borthomieu, C. Delmas and C. Fouassier, *J. Power Sources*, 1991, **36**, 113.
21 P. Genin, A. Delahaye-Vidal, F. Portemer, K. Tekaia-Elhsissen and M. Figlarz, *Eur. J. Solid State Inorg. Chem.*, 1991, **28**, 505.
22 C. Hennig, K. H. Hallmeier, G. Zahn, F. Tschwatschal and H. Hennig, *Inorg. Chem.*, 1999, **38**, 38.
23 M. Takahashi, H. Tanida, S. Kawauchi, M. Harada and I. Watanabe, *J. Synchrotron Radiat.*, 1999, **6**, 278.
24 J. H. Choy, Y. M. Kwon, K. S. Han, S. W. Song and S. H. Chang, *Mater. Lett.*, 1998, **34**, 356.
25 S. G. Gurman, N. Binsted and I. Ross, *J. Phys. C*, 1984, **C17**, 143.
26 S. G. Gurman, N. Binsted and I. Ross, *J. Phys. C*, 1986, **C19**, 1845.
27 K. I. Pandya, W. E. O'Grady, D. A. Corrigan, J. McBreen and R. W. Hoffman, *J. Phys. Chem.*, 1990, **94**, 21.
28 B. C. Cornilsen, X. Shan and P. L. Loyselle, *Proc. Electrochem. Soc.*, 1990, **90-4**, 82.
29 A. N. Mansour and C. A. Melendres, *J. Phys. Chem. A*, 1998, **102**, 65.
30 R. Allman, *Z. Kristallogr.*, 1968, **126**, 417.
31 W. Stählin and H. R. Oswald, *Acta Crystallogr., Sect. B*, 1970, **B26**, 860.
32 R. D. Shannon and C. T. Prewitt, *Acta Crystallogr., Sect. B*, 1969, **B25**, 925.
33 R. J. Doran, *Proceedings of the International Symposium on Batteries*, Royal Aircraft Establishment, Farnborough, Hampshire, UK, 1958, Paper (y).
34 A. Mendiboure and R. Schöllhorn, *Rev. Chim. Miner.*, 1986, **23**, 819.
35 A. D. Wadsley, *Acta Crystallogr.*, 1955, **8**, 165.
36 S. Yamanaka, K. Ando and M. Ohashi, *Mater. Res. Soc. Symp. Proc.*, 1995, **371**, 131.
37 H. Nishizawa and K. Yuasa, *J. Solid State Chem.*, 1998, **141**, 229.